communications earth & environment

Article

https://doi.org/10.1038/s43247-024-01559-5

Arctic sea ice loss warmed the temperate East Asian winter in the mid-Holocene

Check for updates

Jiang Dong[1,2], Xuefa Shi[1,2] ✉, Haijin Dai[3] ✉, Zhengyao Lu[4] ✉, Xiting Liu[5], Anatolii S. Astakhov[6], Limin Hu[5], Gang Yang[1], Yuri Vasilenko[6], Alexander Bosin[6], Jingjing Gao[1], Yanguang Liu[1,2], Jianjun Zou[1,2], Zhengquan Yao[1,2] & Anchun Li[7]

The recent colder winters in midlatitude Eurasia have been proposed to result from Arctic sea-ice decline. However, large uncertainties remain regarding this link in the present variable climate. Here, we present ice-rafted debris records from the eastern Arctic and geochemical data from the temperate East China Sea to reconstruct Holocene changes in sea ice and the East Asian winter monsoon. Our reconstructions and climate numerical simulations revealed enhanced Arctic sea-ice decline but warmer winters in East Asia in the mid-Holocene than in the late Holocene. In the warmer mid-Holocene, enhanced Arctic sea-ice loss transferred more heat from intensive summer solar insolation to the winter atmosphere, suppressing meridional heat transport; thus, less high-latitude cold air moved to lower latitudes in Asia due to the weakened winter monsoon. Our findings imply that the colder winters in East Asia may not change the long-term trend toward winter warming in the context of Arctic sea-ice decline.

The present ongoing warming is accompanied by rapid Arctic sea ice decline and subsequently influences the global climate and triggers extreme climate events[1–3]. A contrasting change between the rapid retreat of summer/autumn Arctic sea ice and the colder winter in midlatitude Eurasia has been unexpectedly observed in the last two decades against the background of long-term global warming[4], which is referred to as the "warm Arctic–cold continents" climate pattern[5,6] (Fig. 1a). Regression analysis and climate simulation studies have attributed the colder winter in midlatitude Eurasia to the rapid decline in Arctic sea ice, likely through planetary waves, storms, and/or jet streams[5–7]. However, this link remains under debate due largely to the limited observation records with large internal variability within the Arctic and midlatitude climate systems and/or intermittency of the teleconnections[8,9]. In addition, this link is also complicated by climate change at lower latitudes, present human activities accompanied by increased greenhouse gas concentrations, and the lagged influences of the prior state of ocean-atmospheric circulation[10,11]. Beyond these limited observations, paleoclimate changes during the warm period of the mid-Holocene (8.2–4.2 ka) can elucidate the effect of Arctic sea ice decline on the midlatitude winter climate under a long-term global warming background.

In the mid-Holocene, proxy-based quantitative reconstructions indicate that the summer insolation-driven global temperature was warmer than that in the late Holocene and recent decades[12]. Because of Arctic amplification, Arctic warming was prominent[13], and the decline in Arctic sea ice might have intensified during this warm period[14,15]. Thus, this warm condition in the mid-Holocene without substantial impacts from human activities is an interesting and natural experiment to investigate[16,17]. On the one hand, statistical analyses and models indicate that the decline in the equator-to-pole meridional temperature gradient due to Arctic amplification possibly results in a more stable climate in warm intervals than in cold intervals[18,19]. As a result, the weaker variances of proxy records in sea ice and Asian climate in the mid-Holocene than in the late Holocene imply that the relatively weak variabilities on millennial timescales can largely limit the influences of internal variabilities and the lagged influences of prior atmospheric state dependence[20–22]. On the other hand, the winter climate in the cooling core area (i.e., Central Asia and Siberia) is mostly controlled by the Siberian High and the East Asian Trough (Fig. 1a). Although we cannot directly reconstruct the midlatitude winter surface air temperature, the strength of the East Asian winter monsoon (EAWM) can alternatively indicate the East and Central Asian winter temperatures. The EAWM

[1]Key Laboratory of Marine Geology and Metallogeny, First Institute of Oceanography, Ministry of Natural Resources, Qingdao, China. [2]Laboratory for Marine Geology, Qingdao Marine Science and Technology Center, Qingdao, China. [3]College of Meteorology and Oceanography, National University of Defense Technology, Changsha, China. [4]Department of Physical Geography and Ecosystem Science, Lund University, Lund, Sweden. [5]Key Laboratory of Submarine Geoscience and Prospecting Techniques, College of Marine Geosciences, Ocean University of China, Qingdao, China. [6]V.I. Il'ichev Pacific Oceanological Institute, Far Eastern Branch of Russian Academy of Sciences, Vladivostok, Russia. [7]Key Laboratory of Marine Geology and Environment, Institute of Oceanology, Chinese Academy of Sciences, Qingdao, China. ✉e-mail: xfshi@fio.org.cn; hj_dai@nudt.edu.cn; zhengyao.lu@nateko.lu.se

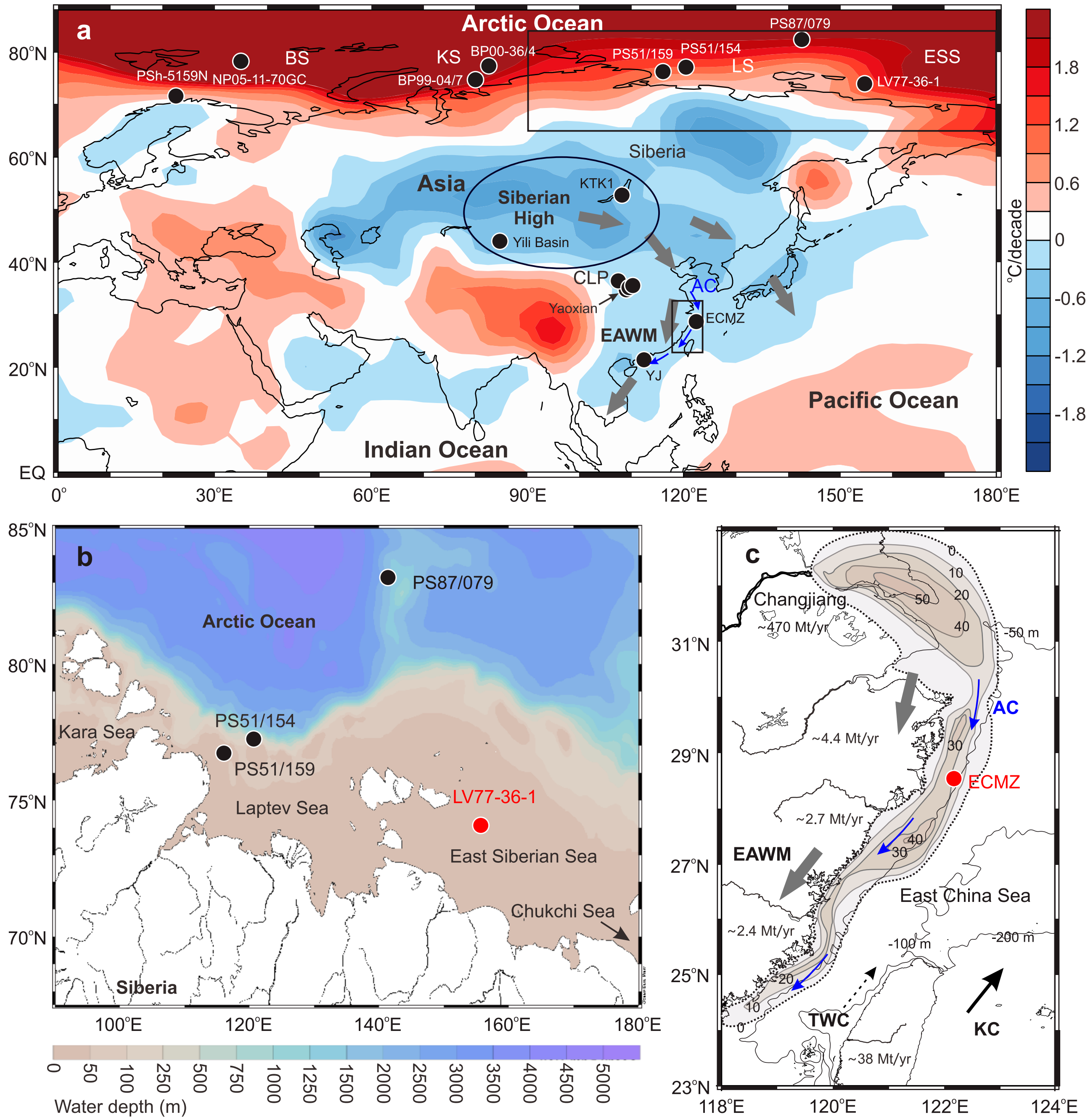

Fig. 1 | Observations of Arctic warming and midlatitude Eurasian colder winters with insets showing the East Siberian Sea and the East China Sea. a Linear trend of surface air temperatures in Arctic and Asian winter (December–February) from A.D. 1989–1990 to 2017–2018. Data from the NCEP reanalysis dataset of surface air temperature[4] (https://psl.noaa.gov/). **b**, **c** Core locations in the eastern Arctic Ocean (upper rectangle in **a**) and East China Sea (bottom rectangle in **a**), respectively. The red and black dots are the gravity cores in this study and the reference cores, respectively. The mean annual major river sediment load[36], winter ocean currents (lines with arrows)[34], and spatial distribution of the Changjiang River discharged material-dominated distal mud in the Holocene (shaded area, in meters)[35], the East Asian winter monsoon (EAWM, gray arrows), and the locations of the Siberian High (circle), Chinese Loess Plateau (CLP), Barents Sea (BS), Kara Sea (KS), Laptev Sea (LS), and East Siberian Sea (ESS) are also shown. The major ocean currents in the East China Sea include the Kuroshio Current (KC), Taiwan warm current (TWC), and alongshore current (AC). The TWC is shown as the dotted arrow because it cannot flow freely in the northern strait in winter.

originates in the Siberian High and is also substantially influenced by the East Asian Trough, which transports cold and dry air southward, fundamentally dominating the cold or warm winter climate in East Asia[23–25]. In a sense, the EAWM is one of the most important manifestations of the pressure field of the Siberian High and the East Asian Trough. Because the intensity of the EAWM is closely and positively linked with the Siberian High and the East Asian Trough but evolves negatively with the central Asian winter temperature[24,26,27], it can also provide an independent reconstruction of the winter climate evolution in temperate Asia. Overall, we focus on Arctic sea ice and EAWM changes on the millennial timescale of the Holocene, which provides valuable records that may reveal the link between high- and midlatitude winter climates in these regions (Fig. 1a).

In the eastern Arctic Ocean, rapid sea ice decline and summer sea ice-free conditions have been accompanied by global warming from the late twentieth century to the present[1,2]. The East Siberian Sea and adjacent seas are some of the most prominent areas in the Arctic where the concentration, coverage, and thickness of seasonal sea ice have decreased, especially in autumn, resulting in stronger autumn and early winter warming than in other Arctic seas[13,28]. Moreover, the East Siberian Sea is an important source region that net exports seasonal sea ice into the Arctic Ocean and influences basin-scale sea ice development[29–31]. Thus, the East Siberian Sea is a representative area for studying Arctic climate changes based on sea ice reconstructions (Fig. 1b). In the East Siberian Sea, ice-rafted detritus (IRD) is primarily concentrated and becomes abundant in sea ice via suspension freezing during sea ice development; thus, the IRD can be used as a proxy for sea ice changes[29–31].

Similarly, the most prominent surface feature of the EAWM is a strong northeasterly wind along the East Asian coasts, and the temperate East China Sea is in the core pathway of the EAWM[24,25] (Fig. 1c). On the East China Sea shelf, the EAWM has driven the alongshore current and has determined its intensity both in the present and during the Holocene[32,33]. In winter, the EAWM develops, and this alongshore current substantially intensifies with a maximum surface velocity of ~50 cm s^{-1}, transporting ~90% of the Changjiang River freshwater southward along the inner shelf over a span of ~1000 km (water depth <50 m), subsequently increasing the suspended sediment concentration by up to >300 mg L^{-1} (refs. 33–36). In the mud area of the East China Sea, long-term observations have recorded positive correlations among the winter northerly wind (i.e., EAWM), the southward alongshore current, and the suspended sediment concentration, but there is a negative link between the northerly wind and surface temperature[37]. In summer, a reversed southerly develops. As a result, the discharge sediment from the Changjiang River is mostly deposited on its delta and transported northeastward[34,35]. The suspended sediment concentration in the East China Sea inner shelf region is <20 mg L^{-1} because of the absence of the EAWM in summer[34]. Thus, the transport and sedimentation of the Changjiang River-dominated suspended material in the East China Sea inner shelf mainly occur in winter. Therefore, based on the mechanical differentiation in suspended sediment due to long-distance transport through the EAWM-driven alongshore current[23], the EAWM can be reconstructed using the Zr/Rb ratio proxy because the elements Zr and Rb are concentrated in coarse-grained and fine-grained sediments, respectively, representing a relatively intensified or weakened alongshore current[27,38].

In this study, we present records of IRD (125–250 μm, grains of individual minerals and rock debris per gram) from Station LV77-36-1 in the East Siberian Sea and Zr/Rb ratios from Station ECMZ in the East China Sea to reconstruct Holocene variations in Arctic sea ice and the EAWM, respectively (Fig. 1b, c, Methods). We focus on the changes in Arctic sea ice and the EAWM from the mid-Holocene (7.5–4.0 ka) to the late Holocene (4.0–0 ka), as reworked and recycled shelf sediments cannot be used to provide useful records in the early Holocene due to rapid sea-level rise[39]. Because seasonal sea ice mainly occurs in the eastern Arctic Ocean and synchronously declines under warming conditions[13,28], we also compared our reconstructions with the overall seasonal sea ice evolution in the eastern Arctic and the winter climate over Central and East Asia during the Holocene based on a compilation of published paleoclimate datasets to reduce the regional limitations of our records (Supplementary Fig. 1). Finally, in comparison to proxy reconstructions, we further applied numerical simulations of the Community Earth System Model Version 1.0 (CESM1.0) and the Coupled Model Intercomparison Project Version 6.0-the paleoclimate Model Intercomparison Project 4 (CMIP6-PMIP4) to model the East Asian winter surface air temperature in the mid-Holocene and reveal the physical processes underlying the influence of the eastern Arctic seasonal sea ice on the EAWM (Methods, Supplementary Method, Supplementary Note, Supplementary Fig. 2).

Our results, combined with a synthesis of the published paleoclimate dataset, reveal a weakened EAWM during the period of enhanced decline in Arctic sea ice in the mid-Holocene, indicating that Arctic sea ice loss could warm temperate Asian winters on millennial timescales. Although our results show conditions contrary to those of short-term observations[6], these findings can help in understanding long-term climate processes in the context of global warming with Arctic sea ice loss.

Results and discussion

Decrease in Arctic sea ice in the mid-Holocene

We first used the IRD proxy to indicate sea ice changes in the East Siberian Sea during the Holocene (Fig. 2a). In the East Siberian Sea Shelf region, the terrigenous minerals and rock debris in the 125–250 μm fractions are interpreted as IRD because the sand fraction (>63 μm) varies independently for the changes in finer fractions, showing different sedimentary processes for these two size fractions[16]. Sediment source analysis indicates that the finer fractions were discharged from local rivers and rapidly deposited, while the sand fraction was enriched in the sea ice through rising frazil with local suspended particles during the Holocene[16,31,40]. In this study, the influence of authigenic minerals and minerals >250 μm are further excluded from our IRD records to minimize the effect of icebergs (commonly indicated by minerals >250 μm) and to focus on Arctic sea ice changes because seasonal sea ice developed in the eastern Arctic through the middle and late Holocene[15].

Since the mid-Holocene, the IRD content has increased (Fig. 2a). Moreover, in both the Chukchi Sea[29] and Fram Strait (juncture between the Atlantic and Arctic Oceans)[30], the chemical compositions of Fe oxides suggest that the amount of East Siberia-sourced ice-rafted iron grains has also increased since the mid-Holocene, and these grains peaked in the late Holocene. Our IRD records are consistent with these ice-rafted iron records, suggesting a decrease in sea ice in the East Siberia Sea and less export by sea-ice transport in the mid-Holocene than in the late Holocene. In adjacent deep sea and shelf areas, dinocysts and biomarker records show the enhanced melting of sea ice and a sporadic occurrence of summer sea ice-free conditions (<50% sea ice cover)[14,15], accompanied by a higher surface air temperature in the mid-Holocene than in the late Holocene[41]. In addition, in the eastern Arctic regions covered by seasonal sea ice, the biomarker IP_{25} and quartz records from the Laptev Sea[42], Kara Sea[43], and Barents Sea[44,45] increased from the mid-Holocene to the present, suggesting stronger melting of sea ice in the eastern Arctic spring and summer in the mid-Holocene than in the late Holocene (Fig. 2a). Therefore, our results, along with the IRD and biomarker records, reveal a synchronous decline in the overall seasonal sea ice in the eastern Arctic in the mid-Holocene (Supplementary Fig. 1), which is consistent with stronger Arctic summer solar insolation in the mid-Holocene than in the late Holocene[46] (Fig. 2b).

Weakened EAWM in the mid-Holocene

We also analyzed the Zr/Rb ratio proxy from the temperate East China Sea to reveal the evolution of the EAWM during the Holocene (Fig. 2b). Against the background of no obvious changes in the regional tidal conditions due to the slight sea level change from the mid-Holocene to the late Holocene[32,39,47], both the Zr/Rb ratio and the grain size data from the East China Sea show similar increasing trends[23]. This increasing trend contrasts with the decreasing changes in East Asian precipitation, the Changjiang River sediment supply, and the river mouth grain size, and it is also different from the typhoon changes[23,32,48]. Thus, based on long-term observations[34,37], the most likely explanation for the Zr/Rb ratio is hydrodynamic differentiation in long-distance transport through the EAWM-driven alongshore current.

In the East China Sea, the low Zr/Rb ratio reveals a weakened alongshore current and thus indicates a weaker EAWM in the mid-Holocene than in the late Holocene (Fig. 2b). Moreover, in the southern sea, organic biomarkers also suggest that more terrigenous biomass was transported southwestward by the stronger alongshore current during the period of decreased river discharge in the late Holocene than during the mid-Holocene, which also points to a weakened (intensified) EAWM in the mid-Holocene (late Holocene)[49] (Fig. 2b). In parallel, multiple land records of loess grain size and dust mass accumulation rate from the midlatitude Asian continents also reveal a weakened EAWM with less variability in the mid-Holocene compared with the late Holocene, which are positively linked to the weakened Siberian High[26,48], but it is negatively related to the higher winter surface air temperature in central Asia and southern Siberia derived from pollen- and mollusk-based reconstructions[22,50] (Fig. 2b). These land records are consistent with marine records, and the reconstructed weakened EAWM also coincides with the relatively high overall winter temperature of the boreal midlatitude continent in the mid-Holocene[51,52]. Overall, the weakened EAWM can reveal warm winter temperatures in East and Central Asia, which occurred coherently with the enhanced decrease in eastern Arctic summer sea ice in the mid-Holocene.

Warm winters in temperate East Asia were driven by Arctic sea ice loss

In the Northern Hemisphere, winter solar insolation became stronger from the mid-Holocene to the present[46] (Fig. 2b). The relatively higher winter solar shortwave forcing would have theoretically warmed the East Asian winter in the late Holocene compared to that in the mid-Holocene[53]. However, the proxy-based reconstructed EAWM has intensified since the mid-Holocene, implying a relatively warm East Asian winter in the mid-Holocene than in the late Holocene (Fig. 2b). In contrast, the central Asian warm winter and weakened EAWM occurred synchronously with the enhanced decline in Arctic sea ice in the mid-Holocene (Fig. 2a, b). Because Arctic sea ice is one of the most important cold air sources of the climate system, this result implies that there were possible close links between the enhanced decline in Arctic sea ice and the EAWM (i.e., East Asian warm winter) in the mid-Holocene.

Previous studies based on Chinese loess records and CESM transient simulations indicated that the intensified EAWM has resulted from decreased annual mean atmospheric temperatures and solar insolation in the middle and high latitudes and increased Arctic sea ice since the mid-Holocene[48,54]. The annual warming in the middle and high latitudes coincided with intensified summer solar insolation, but it was restrained by weakened winter radiation in the mid-Holocene (Fig. 2b). In the Arctic, proxy-based reconstructions of the enhanced decrease in eastern Arctic sea ice occurred mainly in summer and spring, which was primarily driven by intensive summer solar insolation in the mid-Holocene[14,42–44] (Fig. 2). In contrast, Arctic solar insolation was approximately zero in winter throughout the Holocene[46]; thus, the annual Arctic heat flux was also dominated by summer solar insolation. Previous studies based on idealized paleoclimate model simulations have indicated that Arctic summer heat could persist into winter due to the enhanced decline in sea ice and compensate for or even exceed that of weakened solar heat forcing in boreal high and middle latitudes, extending to ~50° N in the mid-Holocene winter[55,56]. Thus, the positive thermal anomaly in Arctic winter due to summer sea ice loss may change the global heat redistribution and related variations in atmospheric circulation, which may have been important in regulating the East Asian winter and the EAWM change in the mid-Holocene.

Our CESM sea ice sensitivity simulations modeled the enhanced decline in sea ice in the mid-Holocene to first demonstrate the associated processes of seasonal heat absorption and release (Fig. 3). The magnitude of the Arctic sea ice concentration reduction simulated by the CESM is consistent with the results of a compilation of Arctic sea ice reconstructions, indicating that the summer sea ice decline occurred mainly in the eastern Arctic Ocean (Supplementary Fig. 1). As a result, the eastern Arctic surface

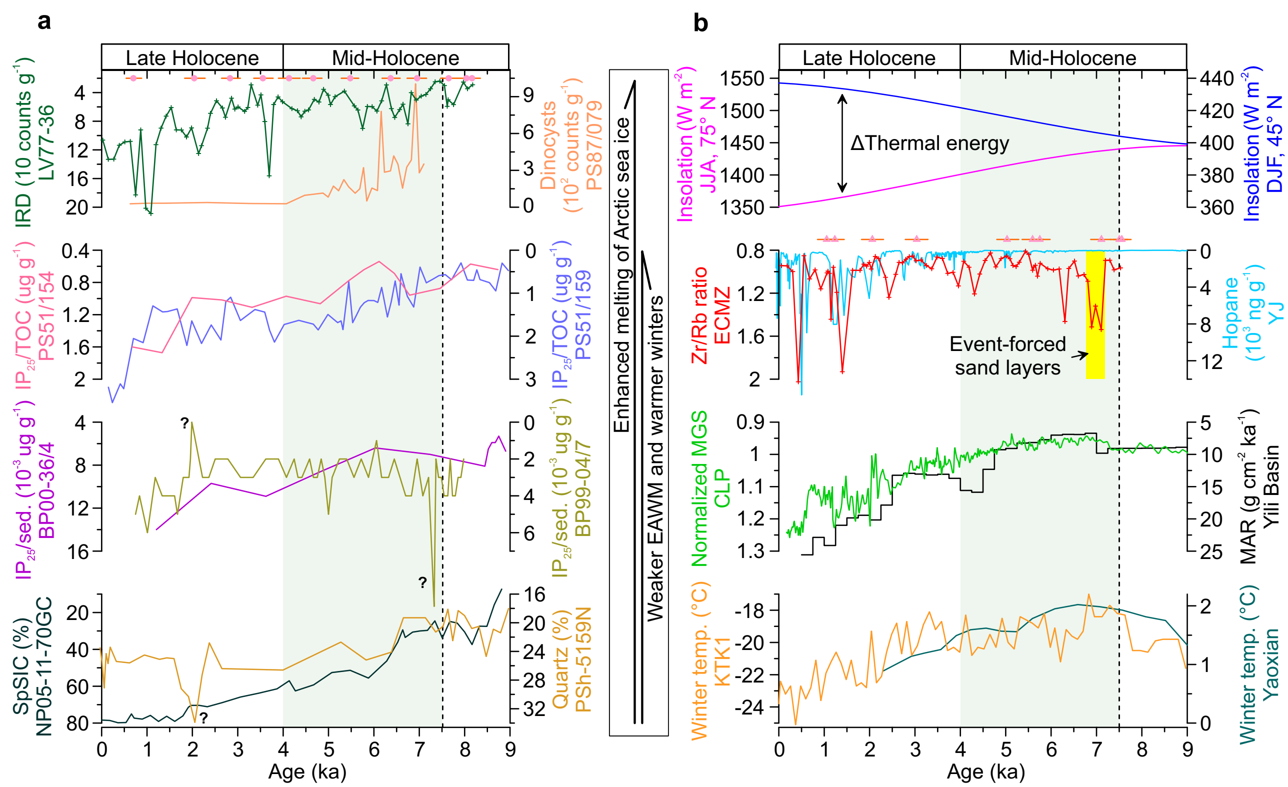

Fig. 2 | Proxy-based Arctic sea ice decline versus temperate Asian warm winters in the mid-Holocene. **a** Reconstruction of the enhanced decline in eastern Arctic sea ice in the mid-Holocene (green band). These reconstructions are based on the IRD in the East Siberian Sea (this study), micropaleontological records in the adjacent deep sea[14], organic geochemical records in the Laptev Sea[42], sea ice biomarkers in the Kara Sea[43], and the quantitative spring sea ice concentration (SpSIC)[44] and quartz percentage in the Barents Sea[45]. **b** Solar insolation and East Asian warm winter in the mid-Holocene. Compared with that in the late Holocene, solar insolation in the Arctic summer (June + July + August, JJA, 75° N) increased, while solar insolation in the midlatitude winter (December + January + February, DJF, 45° N) decreased in the mid-Holocene[46]. The reconstructions of the East Asian winter monsoon (EAWM) and the related weakened Siberian High and midlatitude Asian warm winters are based on geochemical (this study) and organic biomarkers in the East Asian marginal seas[49], the stacked normalized mean grain size (MGS) from the Chinese Loess Plateau (CLP)[48], the stacked dust mass accumulation rate (MAR) from the Yili Basin in central Asia[26], and the quantitative winter surface air temperature based on pollen records from southern Siberia[50] and mollusk data from the CLP[22]. The short lines with dots and triangles are age points with 2-sigma uncertainties. The question marks represent outliers.

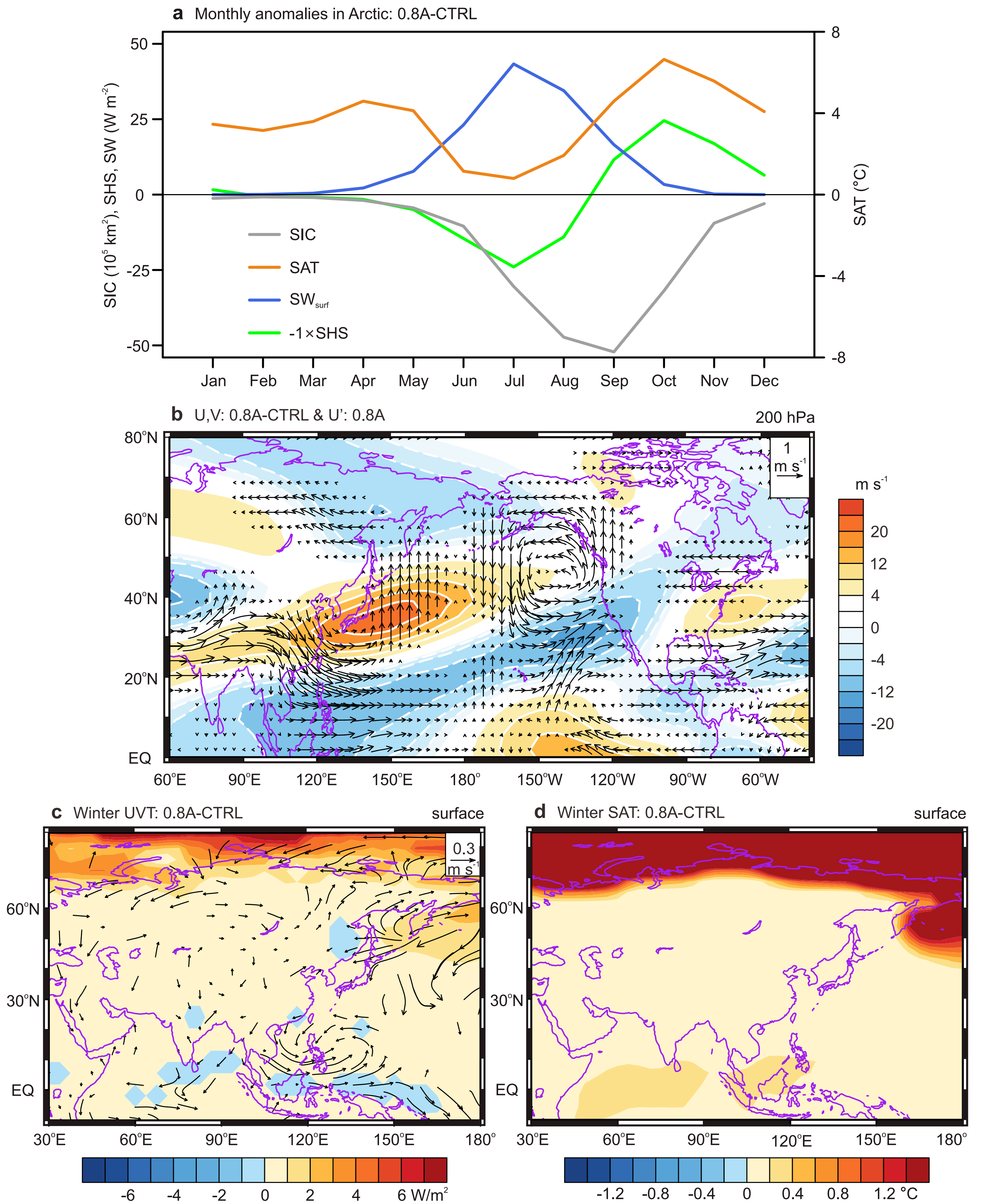

Fig. 3 | Simulated winter heat and air changes due to Arctic sea ice decline. **a** Changes in sea ice (SIC, gray line), surface air temperature (SAT, orange line), short radiation (SW, blue line), and seasonal heat storage (SHS, green line) in Arctic winter. **b** Winter anomaly of the westerly jet (vector) and zonal velocity disturbance (shaded color, indicates the planetary wave) at 200 hPa in the 0.8 A experiment. The significance and comparison of winter zonal velocity disturbance in the 0.8 A and CTRL experiments are shown in Supplementary Fig. 4. **c** Anomalies of surface wind (vector) and heat transport (UVT, shaded color) in winter. **d** Positive anomaly of surface air temperature in winter. All the changes were analyzed with Student's *t* test, with confidence levels greater than 95%.

albedo decreased (Fig. 3a, gray line), and more shortwave radiation was absorbed at the sea surface, which reached a maximum in summer (Fig. 3a, blue line). Most of the additional shortwave radiation was stored in the upper ocean layer and/or in the shelf bottom water, resulting in anomalously increased temperatures from summer to winter in these water layers[2,57], thus forming additional seasonal heat storage (Fig. 3a, green line, Supplementary Fig. 3). The additional seasonal heat storage could have discharged after summer and warmed the surface Arctic, causing Arctic warming to reach its maximum in autumn and winter (Fig. 3a, orange line). In autumn and early winter, additional seasonal heat was released from the upper ocean layer via strong vertical mixing because more water was directly driven by surface winds due to less sea ice cover[58–60] (Fig. 3a, gray line). In mid-late winter, when the eastern Arctic was covered by sea ice, the decreased sea ice thickness due to a longer period of sea ice melting could have also enhanced the release of additional seasonal heat storage from the upper ocean layer via surface upward sensible heat flux, increasing the Arctic winter surface air temperature[61]. Hence, the CESM-simulated results are consistent with observations[2,57], indicating that the enhanced decrease in eastern Arctic sea ice increased the heat flux transferred from the ocean to the atmosphere in the mid-Holocene winter.

Based on the heat transfer across seasons, our results of CESM climate model simulation further verify the influence of the enhanced Arctic sea ice decline on the East Asian warm winter by heat redistribution and related atmospheric changes. Because the simulated degree of eastern Arctic warming agrees well with the pollen-based quantitative reconstructions of the eastern Arctic winter temperature in the mid-Holocene[62], our CESM simulations provide a representative situation in the mid-Holocene. The relatively increased upward release of the eastern Arctic heat flux and the warmer Arctic surface air in winter suppressed the meridional heat transport from low to high latitudes, and more heat was trapped at lower latitudes (Fig. 3b, c). Because the local climate feedbacks at low latitudes were stronger than those at middle latitudes, such as the positive feedbacks of water vapor and cloud feedback[63], a larger (smaller) temperature increase tended to occur at low (middle) latitudes (Fig. 3d). As a result, the increased meridional temperature gradient between the low and middle latitudes intensified the westerlies, which was inferred from the thermal wind theory (Fig. 3b–d). This result can be further supported by the enhanced westerlies in the mid-Holocene, which are indicated by the dust mass accumulation rate and dust grain size in the northwest Pacific Ocean[64,65]. The faster background flow increased the frequency of the quasistationary planetary wave and dampened its activity according to the dispersion relation of the Rossby wave and the energy formula of the Rossby wave, respectively (Fig. 3b, shading, Supplementary Fig. 4). The decreased planetary wave activity weakened the East Asian trough and the Siberian High (Supplementary Fig. 5), resulting in southerly anomalies in northern East Asia and eastern Siberia (north of ~35° N, east of ~115° E) (Fig. 3c). Therefore, the EAWM weakened, and less cold air was carried from the Arctic into the lower latitudes, resulting in warmer winters in East and Central Asia in the mid-Holocene (Figs. 2 and 3d).

Based on the compilation of proxy reconstructions for sea ice, the EAWM, and East and Central Asian winter temperatures in the Holocene, as well as climate model simulations (Figs. 2 and 3), our results contradict observations over the past two decades (Fig. 1a). A previous study using only the same atmosphere model, Community Atmospheric Model Version 5 (CAM5), found that Arctic sea ice decline might cool the midlatitude Asian winter through weakening of the stratospheric polar vortex[66]. However, the winter stratospheric polar vortex is highly nonlinear by itself, and it can also be influenced by multiple factors from different latitudes and solar heat input[10,66]. Arctic warming can also result in stronger westerly winds and a strongly confined polar vortex through deepening the Arctic surface low-pressure center and increasing the midlatitude-Arctic pressure gradient and thus fewer cold outbreaks to the midlatitudes[11]. A result based on a high-resolution transient simulation using a similar method with CAM4 revealed a weakened EAWM that was statistically significant in the mid-Holocene, implying East Asian warmer winter temperatures in the context of Arctic warming in the mid-Holocene than in the late Holocene[54]. In this study, Arctic sea ice and the ocean and atmosphere from different latitudes, including CAM5, but without drastic changes in ocean circulation, were comprehensively analyzed via coupled CESM1.0 sensitivity simulations. Compared with previous findings, our results reveal a "warm Arctic–warm continents" climate pattern and further illustrate the detailed physical processes underlying the function of enhanced Arctic sea ice decline in warming the East Asian winter via wave-mean flow interactions in the mid-Holocene based on coupled simulations and proxy records (Fig. 4).

In addition, we noted that sea ice loss in different Arctic seas (e.g., the Barents-Kara Seas vs. Chukchi-Bering Seas) probably leads to contrasting impacts on tropospheric circulation in the Northern Hemisphere[67]. Thus, there is uncertainty about Arctic-Asian climate links inferred from only single-core Holocene records, although our proxy records are representative of Arctic warming and a weakened EAWM in the mid-Holocene. In this study, to limit this uncertainty and the spatial heterogeneity of the influence of sea ice in different Arctic regions, overall sea ice loss in the eastern Arctic was analyzed in our climate model simulations because of the simultaneous decline in sea ice in the mid-Holocene (Supplementary Fig. 1). Hence, we focus on the overall effect of the decrease in eastern Arctic sea ice on the East Asian winter climate.

Overall, from the perspective of seasonal heat transfer due to the change in Arctic sea ice and its connection to climate processes, the results of synchronous changes in Arctic sea ice loss and the weakened EAWM from the inversion of multiple proxy-based reconstructions and forward modeling of climate simulations suggest that the enhanced decline in Arctic sea ice warmed the East Asian winter on a millennial timescale under mid-Holocene warming conditions (Fig. 4). Although the major reasons for the warm Arctic differ between the mid-Holocene and the present day, the contributions of global climate warming and enhanced Arctic sea ice loss are similar. In the case of the mid-Holocene without the rise of greenhouse gases, our findings highlight the role of enhanced Arctic sea ice decline in inducing East Asian winter warming. These results imply that the observed short-term occurrence of severely cold winters in East Asia may not change the long-term trend toward warming conditions in winter in the context of Arctic sea ice decline. Therefore, our findings have important implications for assessing climate change at middle and high latitudes related to Arctic sea ice decline under warmer-than-present boundary conditions.

Methods

Materials and age models

Two sediment cores were collected in this study. In September 2016, sediment core LV77-36-1 (155.66° E, 74.10° N) was collected in the low-gradient East Siberian Sea shelf region at a water depth of 36.0 m by the vessel R/V "Akademik Lavrentiev". The recovery of this core sediment was 376 cm, and it was mainly composed of mud without obvious sedimentary structures[16]. In September 2015, sediment core ECMZ (122.17° E, 28.5° N) was collected on the temperate East China Sea shelf at a water depth of 40.0 m by the vessel "Kan 407". The length of the upper mud sediment in this core was 1546 cm, and it was also mainly composed of silt and clay[68]. Both core sediments were deposited mainly in a shallow sea environment[16,68]. Notably, event-forced sand layers were identified at lengths between 1450 cm and 1350 cm in the sediment core ECMZ, which was unable to provide useful reconstructions to indicate the alongshore current and related climate changes because they were largely reworked and recycled[32]. Overall, the absence of erosion surfaces and the gradual changes in sediment composition suggest that the mud sediment in both cores was not distinctly affected by reworked or underlying older deposits except at lengths between 1450 cm and 1350 cm in the sediment core ECMZ. Accordingly, the sedimentary strata provide continuous records from the eastern Arctic and temperate East China Sea to reveal the variations in sea ice and the EAWM.

The age models of the core sediments were reconstructed based on accelerator mass spectrometry ^{14}C dating of twelve bivalve shells and ten mixed benthonic foraminifera shells in the 63–250 μm fraction in cores

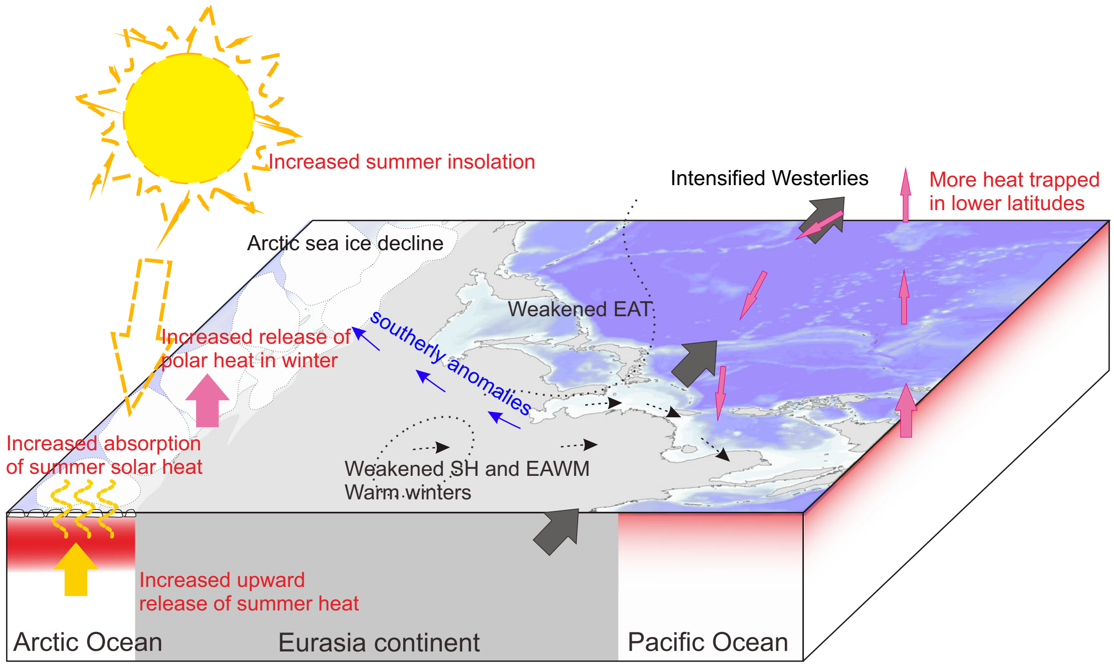

Fig. 4 | Influencing mechanism of Arctic sea ice decline on warm East Asian winters in the mid-Holocene. In the mid-Holocene, the decrease in Arctic sea ice enhanced the absorption of summer solar heat input. This heat was stored in the upper Arctic seawater in summer and released, increasing the heat flux from the ocean to the atmosphere and thus suppressing meridional heat transport from low to high latitudes in winter. As a result, the increased meridional temperature gradient between the low and middle regions intensified the westerlies, suppressing the Rossby wave. This weakened the East Asian trough (EAT) and the Siberian High (SH), generating southerly anomalies. Thus, the temperate Asian winter warmed due to the weakening of the East Asian winter monsoon (EAWM).

LV77-36-1[16] and ECMZ[32], respectively. In this study, we updated the age models based on the Marine 20.14 C dataset via Calib 8.2 software (http://calib.org/calib/)[69]. The local reservoir ages (ΔR) were also referenced in the age calibrations and calculations, which were set at a value of -121 ± 76 years in the temperate East China Sea[70–72] and -95 ± 61 years in the East Siberian Sea and the Laptev Sea[73]. The interpolated ages under a 95% confidence interval were estimated using Clam 2.2 via R software[74]. In addition, the ages of the core surficial sediments (0 cm) were set as the years of core collection based on the ^{210}Pb and ^{137}Cs data[75,76]. The results suggest that both our cores provide sufficient sedimentary records to reconstruct the histories of Arctic sea ice and the EAWM from ~7.5 ka to the present (Supplementary Fig. 6).

IRD
Based on the reconstructed age-depth model of core LV77-36-1, 77 samples at intervals of ~100 years were selected to obtain IRD records. These samples were first dried in an air oven for 48 h at 60 °C and then weighed. Afterward, the samples were water-sieved using a 63 µm mesh. Thus, the coarse fractions (>63 µm) were isolated. These dried coarse fractions were repeatedly sieved using 125 µm and 250 µm meshes. Subsequently, the grains in the 125–250 µm fractions were observed and identified under a ZEISS Stemi 2000 stereoscope with reflected light in the laboratory at the First Institute of Oceanography (Qingdao). In this study, terrigenous individual minerals or rock debris (composed of two or more different minerals) in the 125–250 µm fraction were identified as IRD, while authigenic minerals (e.g., pyrite and gypsum) were not identified as IRD because their formation depends on multiple geochemical and biochemical processes internal to the seas[77,78]. In addition, very coarse grains (>250 µm fractions) were not identified as IRD to indicate seasonal sea ice changes because they were possibly influenced by iceberg transport in geological history[30]. Finally, the number of IRD grains was divided by the corresponding dry unsieved bulk weight to calculate the IRD counts per gram for comparison.

Zr/Rb ratio
Based on the reconstructed age-depth model of the core ECMZ, the geochemical compositions of 76 samples collected at intervals of ~100 years were analyzed to calculate the Zr/Rb ratio. After digesting these bulk samples with a concentrated mixture composed of HNO_3 and HF in Teflon vessels, the element contents were measured by applying a thermal iCAP RQ ICP–MS system at the First Institute of Oceanography. The errors calculated by replicate measurements were <5%.

CESM Arctic sea ice sensitivity simulations
Because Asian climate change could have been remotely influenced by Arctic climate change during the Holocene, we performed sensitivity simulations and prescribed sea-ice parameters in the model simulation to elucidate this remote Arctic forcing, which was relevant to the decline in sea ice. Using the CESM transient simulation, the reconstruction of a weakened EAWM in the mid-Holocene was consistent with proxy records[54], and relatively low Arctic sea ice concentrations could also be simulated by decreased surface albedo to reflect intensive summer solar insolation in the mid-Holocene, which was closely related to heat absorption and transfer across seasons[55,58–60]. In this study, we also employed CESM1.0 to further trace the physical processes of climate variability and change via sensitivity simulations[79], which were composed of a spectral atmospheric model (CAM5, with 26 vertical levels)[80], a land model (CLM4)[81], a tripolar-grid ocean model (POP2, with 60 vertical levels)[82], and a sea-ice model (CICE4)[83]. CESM1.0 was run with a grid spacing of 3.75° for the atmosphere and land models and ~3.0° for the ocean and sea-ice models. Based on the quantitative and semiquantitative reconstructions of Arctic seasonal sea ice, the period of eastern Arctic sea ice cover with >50% concentration in the mid-Holocene was ~0.8 times greater than that in the late Holocene[14,15], and the general ocean circulation did not largely change under this background according to model studies[58–60]. To study the influence of the decrease in eastern Arctic sea ice on the EAWM through heat redistribution and related atmospheric changes, we completed a 2000-year preindustrial control run (CTRL) and a 500-year surface albedo perturbation run (0.8 A) using CESM1.0. During 1501–2000, 0.8 A was “parallel” to CTRL, with the same

initial conditions at the end of 1500, while the surface albedo (for shortwave radiation) over the (global) ice-covered ocean was set to 0.8 times its original value (only the surface albedo in the ocean model was revised artificially). The surface albedo in other parts of the coupled climate model was not revised artificially. CO_2 was fixed at 284.7 ppmv, and all orbital parameters were fixed at preindustrial conditions for simplicity and to focus on the impacts of Arctic sea ice melt. The 0.8 A reached quasiequilibrium after the 500-year integration. Thus, we focused on the equilibrium responses using the monthly averaged fields over the last 200 years of integration. All the changes were analyzed with Student's *t* test, with confidence levels greater than 95%. More importantly, our 0.8 A simulated results coincided well with the proxy-based Arctic sea ice conditions and pollen-based records of eastern Arctic winter temperature anomalies in the mid-Holocene[62] (Supplementary Fig. 1), further increasing the confidence of the CESM simulations of midlatitude Eurasian climate responses to Arctic sea ice in the mid-Holocene.

Data availability

The source data of the marine proxy records in this study are available online at https://doi.org/10.17632/7rhys776cp.1.

Received: 25 January 2024; Accepted: 9 July 2024;
Published online: 24 July 2024

References

1. Comiso, J. C., Parkinson, C. L., Gersten, R. & Stock, L. Accelerated decline in the Arctic sea ice cover. *Geophys. Res. Lett.* **35**, L01703 (2008).
2. Carmack, E. et al. Toward Quantifying the Increasing Role of Oceanic Heat in Sea Ice Loss in the New Arctic. *B. Am. Meteorol. Soc.* **96**, 2079–2105 (2015).
3. Cohen, J., Agel, L., Barlow, M., Garfinkel, C. I. & White, I. Linking Arctic variability and change with extreme winter weather in the United States. *Science* **373**, 1116–1121 (2021).
4. Kalnay, E. et al. The NCEP/NCAR 40-year reanalysis project. *B. Am. Meteorol. Soc.* **77**, 437–471 (1996).
5. Bailey, H. et al. Arctic sea-ice loss fuels extreme European snowfall. *Nat. Geosci.* **14**, 283–288 (2021).
6. Cohen, J. et al. Recent Arctic amplification and extreme mid-latitude weather. *Nat. Geosci.* **7**, 627–637 (2014).
7. Liu, J., Curry, J. A., Wang, H., Song, M. & Horton, R. M. Impact of declining Arctic sea ice on winter snowfall. *Proc. Natl. Acad. Sci. USA.* **109**, 4074–4079 (2012).
8. Cohen, J. et al. Divergent consensuses on Arctic amplification influence on midlatitude severe winter weather. *Nat. Clim. Change* **10**, 20–29 (2019).
9. Screen, J. A. The missing Northern European winter cooling response to Arctic sea ice loss. *Nat. Commun.* **8**, 14603 (2017).
10. Overland, J. E. et al. Nonlinear response of mid-latitude weather to the changing Arctic. *Nat. Clim. Change* **6**, 992–999 (2016).
11. Dai, A. & Song, M. Little influence of Arctic amplification on mid-latitude climate. *Nat. Clim. Change* **10**, 231–237 (2020).
12. Marcott, S. A., Shakun, J. D., Clark, P. U. & Mix, A. C. A reconstruction of regional and global temperature for the past 11,300 years. *Science* **339**, 1198–1201 (2013).
13. Serreze, M. C., Barrett, A. P., Stroeve, J. C., Kindig, D. N. & Holland, M. M. The emergence of surface-based Arctic amplification. *Cryosphere* **3**, 11–19 (2009).
14. de Vernal, A. et al. Natural variability of the Arctic Ocean sea ice during the present interglacial. *Proc. Natl. Acad. Sci. USA.* **117**, 26069–26075 (2020).
15. Stein, R. et al. Holocene variability in sea ice cover, primary production, and Pacific-Water inflow and climate change in the Chukchi and East Siberian Seas (Arctic Ocean). *J. Quaternary Sci.* **32**, 362–379 (2017).
16. Dong, J. et al. Enhanced Arctic sea ice melting controlled by larger heat discharge of mid-Holocene rivers. *Nat. Commun.* **13**, 5368 (2022).
17. Park, H. S. et al. The impact of Arctic sea ice loss on mid-Holocene climate. *Nat. Commun.* **9**, 4571 (2018).
18. Rehfeld, K., Munch, T., Ho, S. L. & Laepple, T. Global patterns of declining temperature variability from the Last Glacial Maximum to the Holocene. *Nature* **554**, 356–359 (2018).
19. Screen, J. A. Arctic amplification decreases temperature variance in northern mid- to high-latitudes. *Nat. Clim. Change* **4**, 577–582 (2014).
20. Zhang, Z. et al. Holocene climatic optimum in the East Asian monsoon region of China defined by climatic stability. *Earth Sci. Rev.* **212**, 103450 (2021).
21. Funder, S. et al. A 10,000-Year Record of Arctic Ocean Sea-Ice Variability—View from the Beach. *Science* **333**, 747–750 (2011).
22. Dong, Y. et al. The Holocene temperature conundrum answered by mollusk records from East Asia. *Nat. Commun.* **13**, 5153 (2022).
23. Dong, J. et al. Millennial-scale interaction between the East Asian winter monsoon and El Niño-related tropical Pacific precipitation in the Holocene. *Palaeogeogr. Palaeoclimatol. Palaeoecol.* **573**, 110442 (2021).
24. Wang, P. et al. The global monsoon across time scales: Mechanisms and outstanding issues. *Earth Sci. Rev.* **174**, 84–121 (2017).
25. Chen, W., Graf, H. F. & Huang, R. H. The interannual variability of East Asian winter monsoon and its relation to the summer monsoon. *Adv. Atmos. Sci.* **17**, 48–60 (2000).
26. Kang, S. et al. Siberian High Modulated Suborbital-Scale Dust Accumulation Changes Over the Past 30 ka in the Eastern Yili Basin, Central Asia. *Paleoceanogr. Paleoclimatol.* **37**, e2021PA004360 (2022).
27. Chen, J. et al. Zr/Rb ratio in the Chinese loess sequences and its implication for changes in the East Asian winter monsoon strength. *Geochim. Cosmochim. Ac.* **70**, 1471–1482 (2006).
28. Stroeve, J. & Notz, D. Changing state of Arctic sea ice across all seasons. *Environ. Res. Lett.* **13**, 103001 (2018).
29. Darby, D. A., Ortiz, J. D., Grosch, C. E. & Lund, S. P. 1,500-year cycle in the Arctic Oscillation identified in Holocene Arctic sea-ice drift. *Nat. Geosci.* **5**, 897–900 (2012).
30. Darby, D. A., Bischof, J. F., Spielhagen, R. F., Marshall, S. A. & Herman, S. W. Arctic ice export events and their potential impact on global climate during the late Pleistocene. *Paleoceanography* **17**, 15−11−15−17 (2002).
31. Nürnberg, D. et al. Sediments in Arctic sea ice: Implications for entrainment, transport and release. *Mar. Geol.* **119**, 185–214 (1994).
32. Dong, J. et al. Holocene Climate Modulates Mud Supply, Transport, and Sedimentation on the East China Sea Shelf. *J. Geophys. Res. Earth Surf.* **125**, e2020JF005731 (2020).
33. Wu, H. et al. Detiding Measurement on Transport of the Changjiang-Derived Buoyant Coastal Current. *J. Phys. Oceanogr.* **43**, 2388–2399 (2013).
34. Li, G. X. et al. Hydrodynamic condition and suspended sediment diffusion in the Yellow Sea and East China Sea. *J. Geophys. Res. Oceans* **121**, 6204–6222 (2016).
35. Liu, J. P. et al. Flux and fate of Yangtze River sediment delivered to the East China Sea. *Geomorphology* **85**, 208–224 (2007).
36. Milliman, J. D. & Farnsworth, K. L. *River Discharge to the Coastal Ocean: A Global Synthesis* (Cambridge Univ. Press, 2013).
37. Liu, J. T. et al. A comprehensive sediment dynamics study of a major mud belt system on the inner shelf along an energetic coast. *Sci. Rep.* **8**, 4229 (2018).
38. Liu, X. et al. Centennial- to millennial-scale monsoon changes since the last deglaciation linked to solar activities and North Atlantic cooling. *Clim. Past.* **16**, 315–324 (2020).
39. Lambeck, K., Rouby, H., Purcell, A., Sun, Y. Y. & Sambridge, M. Sea level and global ice volumes from the Last Glacial Maximum to the Holocene. *Proc. Natl. Acad. Sci. USA.* **111**, 15296–15303 (2014).

40. Reimnitz, E., Clayton, J. R., Kempema, E. W., Payne, J. R. & Weber, W. S. Interaction of rising frazil with suspended panicles: tank experiments with applications to nature. *Cold Reg. Sci. Technol.* **21**, 117–135 (1993).
41. Routson, C. C. et al. Mid-latitude net precipitation decreased with Arctic warming during the Holocene. *Nature* **568**, 83–87 (2019).
42. Hörner, T., Stein, R., Fahl, K. & Birgel, D. Post-glacial variability of sea ice cover, river run-off and biological production in the western Laptev Sea (Arctic Ocean)—A high-resolution biomarker study. *Quaternary Sci. Rev.* **143**, 133–149 (2016).
43. Hörner, T., Stein, R. & Fahl, K. Paleo-sea ice distribution and polynya variability on the Kara Sea shelf during the last 12 ka. *arktos* **4**, 1–16 (2018).
44. Berben, S. M. P., Husum, K., Navarro-Rodriguez, A., Belt, S. T. & Aagaard-Sørensen, S. Semi-quantitative reconstruction of early to late Holocene spring and summer sea ice conditions in the northern Barents Sea. *J. Quaternary Sci.* **32**, 587–603 (2017).
45. Risebrobakken, B., Moros, M., Ivanova, E. V., Chistyakova, N. & Rosenberg, R. Climate and oceanographic variability in the SW Barents Sea during the Holocene. *Holocene* **20**, 609–621 (2010).
46. Laskar, J. et al. A long-term numerical solution for the insolation quantities of the Earth. *Astron. Astrophys.* **428**, 261–285 (2004).
47. Uehara, K. & Saito, Y. Late Quaternary evolution of the Yellow/East China Sea tidal regime and its impacts on sediments dispersal and seafloor morphology. *Sediment. Geol.* **162**, 25–38 (2003).
48. Kang, S. et al. Early Holocene weakening and mid- to late Holocene strengthening of the East Asian winter monsoon. *Geology* **48**, 1043–1047 (2020).
49. Zhang, Y. et al. Asian Winter Monsoon Imprint on Holocene SST Changes at the Northern Coast of the South China Sea. *Geophys. Res. Lett.* **46**, 13363–13370 (2019).
50. Tarasov, P. E., Bezrukova, E. V. & Krivonogov, S. K. Late Glacial and Holocene changes in vegetation cover and climate in southern Siberia derived from a 15 kyr long pollen record from Lake Kotokel. *Clim. Past.* **5**, 285–295 (2009).
51. Zhang, W. et al. Holocene seasonal temperature evolution and spatial variability over the Northern Hemisphere landmass. *Nat. Commun.* **13**, 5334 (2022).
52. Cartapanis, O., Jonkers, L., Moffa-Sanchez, P., Jaccard, S. L. & de Vernal, A. Complex spatio-temporal structure of the Holocene Thermal Maximum. *Nat. Commun.* **13**, 5662 (2022).
53. Meyer, H. et al. Long-term winter warming trend in the Siberian Arctic during the mid- to late Holocene. *Nat. Geosci.* **8**, 122–125 (2015).
54. Zhou, P. et al. Strengthened East Asian Winter Monsoon Regulated by Insolation and Arctic Sea Ice Since the Middle Holocene. *Geophys. Res. Lett.* **50**, e2023GL105440 (2023).
55. Park, H. S., Kim, S. J., Stewart, A. L., Son, S. W. & Seo, K. H. Mid-Holocene Northern Hemisphere warming driven by Arctic amplification. *Sci. Adv.* **5**, eaax8203 (2019).
56. Bader, J. et al. Global temperature modes shed light on the Holocene temperature conundrum. *Nat. Commun.* **11**, 4726 (2020).
57. Janout, M. et al. Episodic warming of near-bottom waters under the Arctic sea ice on the central Laptev Sea shelf. *Geophys. Res. Lett.* **43**, 264–272 (2016).
58. Dai, H., Zhao, J., Zhao, W., Huang, H. & Liu, Y. Role of Vertical Mixing in the Upper Ocean in the Seasonal Variation of Arctic Amplification. *J. Geophys. Res. Atmo.* **127**, e2022JD037467 (2022).
59. Dai, H. Roles of Surface Albedo, Surface Temperature and Carbon Dioxide in the Seasonal Variation of Arctic Amplification. *Geophys. Res. Lett.* **48**, e2020GL090301 (2021).
60. Dai, H., Zhao, J., Yao, Q. & Zhang, X. The Seesaw of Seasonal Precipitation Variability Between North China and the Southwest United States: A Response to Arctic Amplification. *J. Geophys. Res. Atmo.* **126**, e2020JD034039 (2021).
61. Branson, M. D., Randall, D. A. & Burt, M. A. Dark Warming. *J. Climate* **29**, 705–719 (2016).
62. Andreev, A. A. & Klimanov, V. A. Quantitative Holocene climatic reconstruction from Arctic Russia. *J. Paleolimnol.* **24**, 81–91 (2000).
63. Held, I. M. & Soden, B. J. Water Vapor Feedback and Global Warming. *Annu. Rev. Energ. Env.* **25**, 441–475 (2000).
64. Rea, D. K. & Leinen, M. Asian aridity and the zonal westerlies: Late Pleistocene and Holocene record of eolian deposition in the northwest Pacific Ocean. *Palaeogeogr. Palaeoclimatol. Palaeoecol.* **66**, 1–8 (1988).
65. Dong, Z. et al. Evolution of westerly jet during the last 60 ka: Evidence from core deposits in the central Japan (East) Sea. *Chin. Sci. Bull.* **62**, 1172–1184 (2017).
66. Kim, B.-M. et al. Weakening of the stratospheric polar vortex by Arctic sea-ice loss. *Nat. Commun.* **5**, 4646 (2014).
67. McKenna, C. M., Bracegirdle, T. J., Shuckburgh, E. F., Haynes, P. H. & Joshi, M. M. Arctic Sea ice loss in different regions leads to contrasting Northern Hemisphere impacts. *Geophys. Res. Lett.* **45**, 945–954 (2018).
68. Dong, J. et al. Sea-level oscillations in the East China Sea and their implications for global seawater redistribution during 14.0–10.0 kyr BP. *Palaeogeogr. Palaeoclimatol. Palaeoecol.* **511**, 298–308 (2018).
69. Heaton, T. J. et al. Marine20—the Marine Radiocarbon Age Calibration Curve (0–55,000 Cal Bp). *Radiocarbon* **00**, 1–42 (2020).
70. Hirabayashi, S., Yokoyama, Y., Suzuki, A., Miyairi, Y. & Aze, T. Short-term fluctuations in regional radiocarbon reservoir age recorded in coral skeletons from the Ryukyu Islands in the north-western Pacific. *J. Quaternary Sci.* **32**, 1–6 (2017).
71. Hideshima, S., Matsumoto, E., Abe, O. & Kitagawa, H. Northwest Pacific Marine Reservoir Correction Estimated from Annually Banded Coral from Ishigaki Island, *Southern Japan*. *Radiocarbon* **43**, 473–476 (2001).
72. Yoneda, M. et al. Radiocarbon marine reservoir ages in the western Pacific estimated by pre-bomb molluscan shells. *Nucl. Instrum. Methods Phys. Res. B.* **259**, 432–437 (2007).
73. Bauch, H. A. et al. Chronology of the Holocene transgression at the North Siberian margin. *Global Planet. Change* **31**, 125–139 (2001).
74. Blaauw, M. Methods and code for 'classical' age-modelling of radiocarbon sequences. *Quat. Geochronol.* **5**, 512–518 (2010).
75. Astakhov, A. S. et al. The Role of Ice Cover in the Formation of Bottom Sediment Chemical Composition on the East Siberian Shelf. *Geochemistry International* **59**, 585–598 (2021).
76. Qiao, S. et al. Sediment accumulation and budget in the Bohai Sea, Yellow Sea and East China Sea. *Mar. Geol.* **390**, 270–281 (2017).
77. Liu, X. et al. Pyrite sulfur isotopes constrained by sedimentation rates: Evidence from sediments on the East China Sea inner shelf since the late Pleistocene. *Chem. Geol.* **505**, 66–75 (2019).
78. Liu, X. et al. Nonevaporative origin for gypsum in mud sediments from the East China Sea shelf. *Mar. Chem.* **205**, 90–97 (2018).
79. Hurrell, J. W. et al. The Community Earth System Model: A Framework for Collaborative Research. *B. Am. Meteorol. Soc.* **94**, 1339–1360 (2013).
80. Neale, R. B. et al. *Description of the NCAR community atmosphere model (CAM 5.0)*, NCAR Tech. Notes: NCAR/TN-486+STR (NCAR, 2012).
81. Lawrence, D. M. et al. The CCSM4 Land Simulation, 1850–2005: Assessment of Surface Climate and New Capabilities. *J. Climate.* **25**, 2240–2260 (2012).
82. Smith, R. et al. *The parallel ocean program (POP) reference manual_ Ocean component of the community climate system model (CCSM)*. Tech. Rep. LAUR-10-01853 (Los Alamos National Laboratory, 2010).
83. Hunke, E. C. & Lipscomb, W. H. *CICE: the Los Alamos Sea Ice Model Documentation and Software User's Manual Version 4.1*. Tech. Rep. LA-CC-06-012 (Los Alamos National Laboratory, 2008).

Acknowledgements
We thank the scientific party and technicians of the vessels R/V "Akademik Lavrentiev" and "Kan 407" for obtaining the samples. Permissions for collecting marine cores and sampling were obtained from the First Institute of Oceanography by coauthor Dr. Xuefa Shi, the V.I. Il'ichev Pacific Oceanological Institute, the Far Eastern Branch of the Russian Academy of Sciences by coauthors Dr. Anatolii S. Astakhov, Dr. Yuri Vasilenko, Dr. Alexander Bosin, and the Institute of Oceanology, Chinese Academy of Sciences by coauthor Dr. Anchun Li. This study was funded by the National Key Research and Development Program of China (Grant No. 2023YFF0804600), the Basic Scientific Fund for National Public Research Institutes of China (Grant No. 2023Q06), the National Natural Science Foundation of China (Grant No. 42006199, 42130412), the Shandong Provincial Natural Science Foundation (Grant No. ZR2020QD110), the Swedish Research Council Vetenskapsrådet (Grant No. 2022-03617), and the Ministry of Science and Higher Education (Project No. 121021700342-9).

Author contributions
J.D. proposed the concept, initiated this study, and performed the data analysis. X.S. organized the cruise and sample collection and designed the study. H.D. and Z.L. ran the simulations and interpreted the physical process. J.D., H.D. and Z.L. wrote the manuscript. X.L., A.A., L.H., G.Y., Y.V., J.G. and A.L. contributed to the data analysis. G.Y. and J.G. collected the samples and performed the laboratory measurements, respectively. J.D., X.S., H.D., Z.L., X.L., A.A., L.H., G.Y., Y.V., A.B., J.G., Y.L., J.Z., Z.Y. and A.L. contributed to the refinement and revision of the paper.

Competing interests
The authors declare no competing interests.

Additional information
Supplementary information The online version contains supplementary material available at https://doi.org/10.1038/s43247-024-01559-5.

Correspondence and requests for materials should be addressed to Xuefa Shi, Haijin Dai or Zhengyao Lu.

Peer review information *Communications Earth & Environment* thanks Judah Cohen and the other, anonymous, reviewer(s) for their contribution to the peer review of this work. Primary Handling Editors: Yiming Wang, Joe Aslin and Aliénor Lavergne. A peer review file is available.